Exotic decays of the 125 GeV Higgs boson at future e⁺e⁻ colliders[*]

Zhen Liu(刘真)[1;1)]   Lian-Tao Wang(王连涛)[2;2)]   Hao Zhang(张昊)[3;3)]

[1] Theoretical Physics Department, Fermilab, Batavia, IL 60510, USA
[2] Kavli Institute for Cosmological Physics and the Enrico Fermi Institute, The University of Chicago, Chicago, IL 60637, USA
[3] Institute of High Energy Physics, Chinese Academy of Sciences, Beijing 100049, China

Abstract: The discovery of unexpected properties of the Higgs boson would offer an intriguing opportunity to shed light on some of the most profound puzzles in particle physics. Beyond Standard Model (BSM) decays of the Higgs boson could reveal new physics in a direct manner. Future electron-positron lepton colliders operating as Higgs factories, including CEPC, FCC-ee and ILC, with the advantages of a clean collider environment and large statistics, could greatly enhance sensitivity in searching for these BSM decays. In this work, we perform a general study of Higgs exotic decays at future e⁺e⁻ lepton colliders, focusing on the Higgs decays with hadronic final states and/or missing energy, which are very challenging for the High-Luminosity program of the Large Hadron Collider (HL-LHC). We show that with simple selection cuts, $\mathcal{O}(10^{-3}-10^{-5})$ limits on the Higgs exotic decay branching fractions can be achieved using the leptonic decaying spectator Z boson in the associated production mode e⁺e⁻ → ZH. We further discuss the interplay between detector performance and Higgs exotic decays, and other possibilities of exotic decays. Our work is a first step in a comprehensive study of Higgs exotic decays at future lepton colliders, which is a key area of Higgs physics that deserves further investigation.

Keywords: Higgs, exotic decay, BSM, lepton collider, Higgs factory

PACS: 12.60.Fr, 13.66.Fg, 14.80.Bn   **DOI:** 10.1088/1674-1137/41/6/063102

1   Introduction

The recent discovery of the Higgs boson by the AT-LAS and CMS experiments at the Large Hadron Collider (LHC) opened a new era of particle physics [1, 2]. The Standard Model (SM)-like Higgs boson has a very deep connection to many profound puzzles of fundamental physics, such as the hierarchy problem and the naturalness problem, the nature of dark matter, the origin of neutrino mass, the origin of the fermion mass hierarchy (the flavor problem), the essence of the electroweak phase transition and electroweak bayrogenesis. Essentially all beyond Standard Model (BSM) solutions to these puzzles, such as supersymmetry (SUSY) [3–5], composite Higgs models [6–9], and grand unified theories [10], predict modifications of the properties of the Higgs boson. Hence, the precise measurements of the properties of this Higgs boson have great potential to shed light on BSM physics.

The HL-LHC will measure many SM model decay modes of the Higgs boson to a relative precision of $\mathcal{O}(10\%)$ [11–15]. The future lepton colliders operating as Higgs factories, with their clean collider environment and large statistics, would measure the Higgs boson couplings to a relative precision of $\mathcal{O}(0.1\% - 1\%)$ [16–18]. Many discussions about the physics potential of future lepton colliders focus on the precision measurement of the Higgs properties in the effective field theory (EFT) framework [19–24]. However, new physics could manifest itself through Higgs exotic decays if some new light degrees of freedom are present, which are not described by the SM EFT. Hence, systematically searching for Higgs exotic decays would be an important physics component of the future lepton collider programs. Moreover, since many of these future facilities are currently at different stages of planning, investigation of these new physics potentials could impact their designs to achieve some more comprehensive physics goals.

1) E-mail: zliu2@fnal.gov
2) E-mail: liantaow@uchicago.edu
3) E-mail: zhanghao@ihep.ac.cn

In Section 2, we present an overview of exotic decay searches at lepton colliders and some general discussions of the Higgs exotic decays at different future lepton colliders. In Section 3, we describe our simulation framework and present our phenomenological analysis for various Higgs exotic decay modes. We summarize the physics potential from the Higgs exotic decays at the (HL-)LHC and the future lepton collider programs in Section 4. In our summary table, we include comprehensive projections and show the complementarity between future lepton collider programs and the HL-LHC. We also discuss many important future directions for the Higgs exotic decay programs.

2   Theoretical framework

2.1   Higgs exotic decay modes considered in this work

The Higgs boson BSM decays have a rich variety of possibilities. To organize this study on Higgs boson BSM decays, we selectively choose a set of phenomenologically driven processes. We focus on two-body Higgs decays into BSM particles, which are allowed to subsequently decay further, up to four-body final states. We only consider the Higgs boson as an CP-even particle. CP-

violation effects would affect various differential distributions, and this demands future study. These processes are well-motivated by SM+singlet extensions, two-Higgs-doublet-models, SUSY models, Higgs portals, gauge extensions of the SM, etc. These assumptions have also been emphasized in the recent overview of Higgs exotic decays [25] and the CERN yellow report [26].

We consider in general that the exotic Higgs decays into BSM particles dubbed as X_i, $h \rightarrow X_1 X_2$. The cascade decay modes are classified into four cases, schematically shown in Fig. 1. We discuss their major physics motivation and features at lepton colliders in order.

<u>h → 2</u>: The X_is in this case are detector-stable and charge-neutral.[1] They could be dark matter candidates. The Higgs portal [27] to dark matter models, including various SUSY light dark matter models [28–38], motivates this BSM search channel. The lepton collider background for this channel are mainly from the process $e^+e^- \rightarrow ZZ \rightarrow Z + \nu\bar{\nu}$ and $e^+e^- \rightarrow W^+W^- \rightarrow l^+l^-\nu\bar{\nu}$. This channel, due to its simplicity and importance, has been studied by most of the future lepton collider programs [16–18] and we will quote these results in our summary table. We include this channel here for completeness. In addition, many of the models that motivate this channel also induce other Higgs exotic decays we consider in this study.
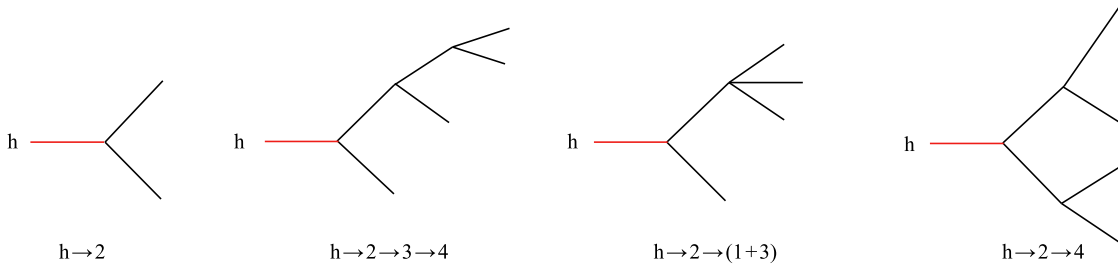

Fig. 1.   The topologies of the SM-like Higgs exotic decays.

<u>h → 2 → 3 → 4</u>: This is the topology in which X_1 is detector-stable and X_2 decays to two particles, with one of these decay products further decaying into two particles. A typical BSM model for such decay modes is the Higgs decaying into the lightest supersymmetric particle (LSP) plus a heavier neutralino, which subsequently decays into the LSP plus a resonant BSM particle. This resonant BSM particle could be a singlet-like scalar in the Next-to-Minimal-Supersymmetric-

Standard-Model (NMSSM). Many SUSY models which motivate Higgs invisible decays also induce this decay channel, e.g. [38, 39]. It also commonly exists in the so-called "stealth SUSY" models [40]. This singlet-like scalar decays into SM fermion pairs, giving rise to the final state of a pair of resonant SM particles plus missing energy, dubbed $h \rightarrow (ff) + \not{E}_T$.[2] In this study, we only consider the channels which are very challenging at the LHC, $h \rightarrow (jj) + \not{E}_T$, $h \rightarrow (b\bar{b}) + \not{E}_T$ and $h \rightarrow (\tau^+\tau^-) + \not{E}_T$.

---

1) The possibility of a detector-stable electrical charged particle X_i is usually more contrived and excluded from direct Drell-Yan production by both LEP and the LHC. Hence, we ignore this possibility here.

2) At lepton colliders we could use the quantity missing momentum instead of Missing Transverse Energy (MET) $\not{E}_T$. The former carries more information while the latter is more widely used in the hadron collider analyses. For the decay channel considered in our analyses, the reach can be improved only marginally by the inclusion of the z-direction missing momentum information because of the already great limit achieved and additional uncertainties from the beamstrahlung effect [41] and the initial state radiation (ISR) effect [42]. Consequently, we use only the more widely adopted missing transverse energy throughout this study.

For the hadronic channels, the major background is from the SM Higgs decay modes $h \to ZZ^* \to jj + \nu\bar{\nu}$ and $h \to ZZ^* \to b\bar{b} + \nu\bar{\nu}$. For $h \to (\tau^+\tau^-) + \not{E}_{\mathrm{T}}$, in addition, the SM Higgs decay $h \to WW^* \to \tau^+\tau^- + \nu\bar{\nu}$ also contributes to the background.

$\underline{h \to 2 \to (1+3)}$: This is the topology when X_1 is detector-stable and X_2 decays into three particles. The typical BSM model is very similar to the previous decay topology. The difference comes from X_2 decaying into three particles without an intermediate on-shell resonance. This scenario takes place very naturally if the singlet-like scalar is heavy, or the particle X_2 decays through an off-shell Higgs or Z-boson. The final state of this Higgs exotic decay signature would be $h \to ff + \not{E}_{\mathrm{T}}$.[1] The lepton collider background sources are similar to the previous topology as well.

$\underline{h \to 2 \to 4}$: In this channel, the Higgs decays to a pair of BSM particles, both of which subsequently decay into two final state particles. There are a wide range of BSM models which give rise to such a decay pattern, and we selectively discuss several benchmark cases. The intermediate particle could be a pair of vectors from the "dark photon" or "dark Z-prime " models [43]. These models commonly include a new gauge boson that couples to the SM with suppressed strength. A typical example is a small kinetic mixing with the hypercharge field strengths, but more general couplings are certainly possible. They not only induce $h \to Z'Z'$ decays but also sizable $h \to ZZ'$ decays in which the masses of the intermediate particles are uneven, if a source of mass mixing is allowed. An important feature of such models relevant for the phenomenology of Higgs exotic decay is that the Z' will have sizable $\mathcal{O}(\text{few}\%)$ decay branching fractions to SM charged leptons. Consequently, this scenario could be severely constrained by the (HL-)LHC searches, unless Z' is leptophobic. This option requires more contrived model building to survives collider direct search limits [44]. The intermediate particle could also be a pair of scalars from SM+scalar, 2HDM+scalar, NMSSM models, etc [25]. In addition, a dark sector with strong dynamics, such as the Twin Higgs [45] models, could also give rise to the Higgs decays into a pair of spin-0 composite particles.[2] The intermediate scalar decays strongly prefer SM heavy fermions and thus $b\bar{b}$, $c\bar{c}$ and $\tau^+\tau^-$ decays would dominate. These decay modes are very hard to probe by (HL-)LHC searches due to the large background in the hadron collider environment. There is the interesting possibility for the intermediate scalars to decay into diphoton pairs that we consider

as well. Hence, we consider many combinations of the $(b\bar{b})$, $(c\bar{c})$, (jj), $(\tau^+\tau^-)$ and $(\gamma\gamma)$ decays of the intermediate particles. The backgrounds are again mainly from SM Higgs decays into four particles through SM gauge bosons. For final states involving photons, the SM electroweak process at the lepton colliders dominates the background.

There are several other decay topologies in Ref. [25] that we do not include in our current study. We comment on them here. $\underline{h \to 2 \to 3}$: In this case, X_1 is detector-stable and X_2 decays promptly. For instance, in dark photon models the SM Higgs decays into $h \to \gamma Z'$ and Z' could subsequently decay into SM particles via two-body decay. In certain SUSY scenarios, the Higgs could decay to the LSP and the next-to-lightest-supersymmetric-particle, which subsequently decays into a photon plus the LSP. $\underline{h \to 2 \to 4 \to 6}$ and $\underline{h \to 2 \to 6}$: the direct decay product from the Higgs undergoes a decay chain or decays into a three-body final state. These decay topologies are common for (R-parity-violating) SUSY models. These decay modes are well-motivated and should be studied in follow-up works.

2.2   Higgsstrahlung process

For future lepton colliders running at the center of mass energy 240–250 GeV, the most important Higgs production mechanism is Z-Higgs associated production through an off-shell Z boson $e^+e^- \to Z^* \to Zh$. The Z boson with visible decays plays the role of Higgs spectator and enables Higgs tagging using the "recoil mass" technique. Given the known initial state energy[3], subtracting the Z-boson four-momentum enables the reconstruction of the Higgs four-momentum and thus its invariant mass. The so called recoil mass defined in this way sharply peaks at the Higgs boson mass. A selection cut around this peak would remove the majority of the SM background.

For an unpolarized electron-positron beam at the center of mass energy 240 GeV, the Higgs production rate is around 230 fb [46, 47]. Both the CEPC and FCC-ee plan to mainly run with unpolarized beam at this energy. Here, we consider the CEPC running scenario with an effective integrated luminosity of 5 ab^{-1}, following its current plan of two interaction points and ten years of running with the designed beam luminosity. The CEPC will produce 1.15 million Higgs bosons in this production channel. The FCC-ee running scenario we consider here has six times more statistics than the

---

1) To explicitly distinguish Higgs exotic decays with or without resonances in the final state particles, we put the pair of SM particles that form a resonance in parenthesis. We follow this notation in describing Higgs exotic decay final states throughout this study.

2) However, in many cases, this composite particle "glu-ball" would be meta-stable and requires a more sophisticated phenomenological study for displaced decays.

3) Corrections from beamstrahlung effect [41] and ISR effect [42] need to be carefully taken into account

CEPC, 30 ab^{-1} (equivalently 6.9 million Higgs bosons), following its current plan of four interaction points with a higher beam luminosity. For the ILC, we only consider the limits from its 250 GeV runs, in the H20 scenario of 2 ab^{-1} integrated luminosity with beam polarization of $p(e^-, e^+) = (-0.8, +0.3)$. The Higgs production rate is enhanced by a factor 1.4 due to beam polarization compared to the unpolarized beams of circular lepton colliders. In this scenario, considering the 250 GeV runs alone, the ILC will produce 0.64 million Higgs bosons in this channel.

Before proceeding to the next section of detailed numerical analysis for individual channels, we comment on several instructive scenarios for the future lepton collider sensitivities here. If we consider the cleanest $e^+e^- \to Zh, Z \to l^+l^-$ mode, the Higgs boson can be tagged with little background from the SM. Taking this leptonic-decaying spectator Z-boson alone and CEPC as an example, we will have 7.7×10^4 Higgs bosons, naively reaching a very impressive 4×10^{-5} (2.5×10^{-4}) limit on the Higgs exotic branching fraction for the case of zero (one hundred) SM background. In this study, we choose to study this clean leptonic spectator Z-boson mode with various Higgs exotic decay modes. For most Higgs exotic decay modes, further inclusion of hadronic decaying Z boson and even invisible Z will definitely improve the limits significantly. The (HL-)LHC will produce more Higgs bosons, providing excellent limits on Higgs decaying into leptons, such as $h \to (l^+l^-)(l^+l^-)$, reaching better than $\mathcal{O}(10^{-5})$ branching fractions. Hence, we do not consider these pure leptonic channels at future lepton colliders but focusing only on the channels that are hard for the LHC, involving hadronic decays and/or missing energy.

3   Phenomenological analysis

Following the discussion in the previous section, we perform a numerical study of the future lepton collider reach for selected Higgs exotic decay modes. Though operating at slightly different center of mass energies in the range of $240-250$ GeV, the proposed future lepton colliders in general have similar detector performance. For simplicity, we choose the CEPC as the benchmark accelerator and detector model in this section for the analysis. We will extrapolate the sensitivity for FCC and ILC in the next section.

For numerical analyses, we generate both the signal and the background events for an 240 GeV electron-positron collider with MadGraph5 at parton level [48] and impose the detector acceptance, energy and momentum smearing, and separation cuts with our own analysis code.

We describe here our parameter choices for the de-

tector effects, and our pre-selection cuts that are universal for the analyses for all Higgs exotic decay mode. To reach a high particle identification efficiency, all of the visible particles in the final state are required to have $|\cos\theta| < 0.98$ (following Ref. [16]), or equivalently $|\eta| < 2.3$. The final state particles are required to be well separated with

$$y_{ij} \equiv \frac{2\min\left(E_i^2, E_j^2\right)\left(1-\cos\theta_{ij}\right)}{E_{vis}^2} \geqslant 0.001. \qquad (1)$$

We only study the case where the Z boson decays into l^+l^- final state where $l^\pm = e^\pm, \mu^\pm$, and leave the study of other decay modes of the Z boson for future works. The signal events are required to contain at least a pair of opposite-sign same-flavor charged leptons with an opening angle greater than $80°$, and satisfy

$$E_l > 5 \text{ GeV} \qquad (2)$$

and

$$|m_{ll} - m_Z| < 10 \text{ GeV}. \qquad (3)$$

Furthermore, the recoil mass is defined as

$$m_{\text{recoil}} \equiv \sqrt{s - 2\sqrt{s}E_{ll} + m_{ll}^2} \qquad (4)$$

where $E_{ll} = E_{l^+} + E_{l^-}$. The recoil mass is required to satisfy

$$|m_{\text{recoil}} - m_h| < 5 \text{ GeV}. \qquad (5)$$

To suppress the ISR contribution to the backgrounds, for Higgs exotic decay modes without missing energy, we require the events to have the total visible energy

$$E_{\text{vis}} > 225 \text{ GeV}. \qquad (6)$$

In this work, we mimic the detector resolution effect by adding Gaussian smearing effects on the four-momentum of the particles, following the performance described in Ref. [16]. For photons in the final state, the energy resolution is determined by the electromagnetic calorimeter, which performs approximately as

$$\frac{\delta E}{E} = \frac{0.16}{\sqrt{E/\text{GeV}}} \oplus 0.01. \qquad (7)$$

The energy resolution of jets is affected by the hadron calorimeter, and performs approximately as

$$\frac{\delta E}{E} = \frac{0.3}{\sqrt{E/\text{GeV}}} \oplus 0.02. \qquad (8)$$

For electrons and muons in the final state, we include the momentum resolution effect of the track system with the approximate performance of

$$\Delta\left(\frac{1}{p_{\mathrm{T}}}\right) = 2 \times 10^{-5} \oplus \frac{10^{-3}}{p_{\mathrm{T}}\sin\theta}. \qquad (9)$$

Next, we discuss the phenomenology of individual Higgs exotic decay channels.

3.1 $h \to (jj) + \not{E}_{\mathrm{T}}$

This final state appears if the SM-like Higgs boson decays into $X_2 X_1$ with $X_2 \to X_1 s$ and $s \to jj$. In the NMSSM, for example, the particles X_1, X_2 and s could be identified as the light neutralinos $\tilde{\chi}_1^0$, $\tilde{\chi}_2^0$ and the light singlet-like (pseudo-)scalar $h_1(a_1)$, respectively. We generate the irreducible SM background $e^+e^- \to l^+l^-\nu_l\bar{\nu}_l jj$ with MadGraph5. Beyond the pre-selection cut and the recoil mass cut, we require that there are two additional jets which satisfy

$$E_j > 10 \text{ GeV and } |\cos\theta_j| < 0.98. \qquad (10)$$

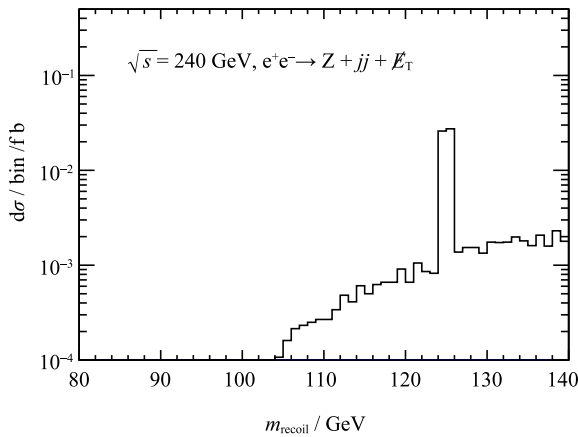After these cuts, the invariant mass distribution of the dilepton system is shown in Fig.2.

Fig. 2.   The recoil mass distribution of the SM backgrounds for $l^+l^-\nu_l\bar{\nu}_l jj$. All of the preliminary cuts except the recoil mass cut are applied.

The dominant background after the recoil mass cut will clearly be the Higgsstrahlung process with $h \to ZZ^* \to q\bar{q}\nu\bar{\nu}$. After the recoil mass cut, the SM background cross section is 0.063 fb.

The dijet invariant mass (m_{jj}) distribution and the two-dimensional differential distribution of m_{jj} versus $\not{E}_{\mathrm{T}}$ of the SM background after the recoil mass cut are shown in Fig. 3. There is a clear valley in the distribution between 35 to 75 GeV, in which none of the Z bosons from the SM-like Higgs boson decay are on-shell and thus the $h \to q\bar{q}\nu_l\bar{\nu}_l$ is doubly suppressed. This property could be used to optimize the cut and increase the sensitivity to the signal if the invariant mass of the light (pseudo)scalar falls in this range.
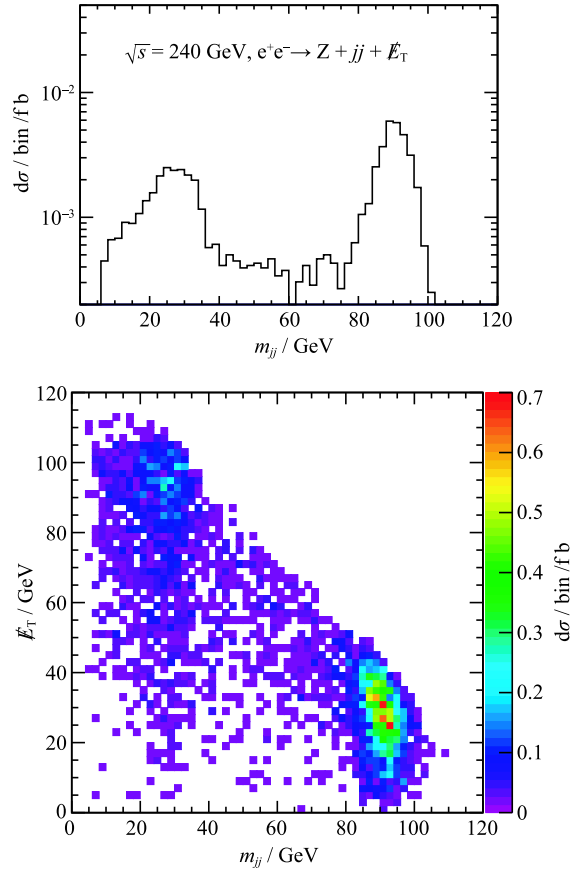

Fig. 3.   (color online) The invariant mass distribution of the SM backgrounds for $l^+l^-\nu_l\bar{\nu}_e jj$ (a), and the m_{jj}-$\not{E}_{\mathrm{T}}$ distribution of the SM backgrounds for $l^+l^-\nu_l\bar{\nu}_l jj$ (b) after cuts.

We use the likelihood function of the m_{jj}-$\not{E}_{\mathrm{T}}$ distribution to give the exclusion limit. We show the 95% C.L. exclusion limit in Fig. 4 in the plane of X_1, mass m_1, and the mass splitting between X_2 and X_1, $m_2 - m_1$, for two benchmark intermediate scalar masses of 10 GeV (a) and 40 GeV (b). In most of the parameter space, the Higgs branching fraction to this exotic decay channel $h \to (jj) + \not{E}_{\mathrm{T}}$ can be excluded to the level of $2 - 6 \times 10^{-4}$. We discuss several kinematical features here that impact the exclusion limit. When $m_s = 10$ GeV, the larger the $m_2 - m_1$, the better the reach. This is due to the fact that the signal events populate the lower-left corner in the m_{jj}-$\not{E}_{\mathrm{T}}$ plane with low SM background for large mass splitting when the MET is small. Consequently, the highest sensitivity is reached when $m_1 = 10$ GeV, $m_2 = 100$ GeV. When $m_2 - m_1$ is small, the signal events will tend to have a large $\not{E}_{\mathrm{T}}$ and look like the SM background events $e^+e^- \to Z(h \to ZZ^*)$ where the on-shell Z from the Higgs boson decay decays to $\nu\bar{\nu}$. Furthermore, for a light intermediate scalar mass, small mass splitting also results in soft jets in the final states which are more likely to fail the pre-selection cuts of two jets. When $m_{h_1} = 40$ GeV (so $m_2 - m_1 \geqslant 40$

GeV), the m_{jj} falls in the valley and the sensitivity is high (around 2×10^{-4}) as we expected. When the intermediate scalar mass m_{h_1} is close to the Z boson mass, the sensitivity is low, due to the relatively large SM background $e^+e^- \to Z(h \to ZZ^*)$ where the on-shell Z from the Higgs boson decay decays to dijets.
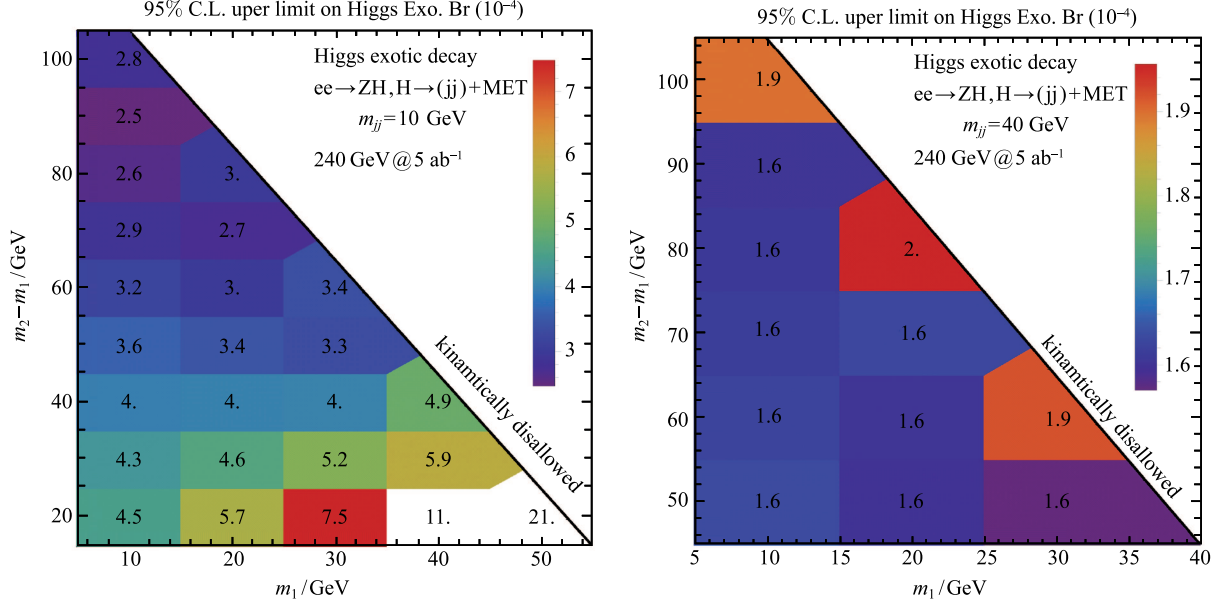

Fig. 4. (color online) The 95% C.L. upper limit on the Higgs exotic decay branching fractions into $(jj) + \not{E}_\mathrm{T}$ for various lightest detector-stable particle X_1 with mass m_1 and mass splittings $m_2 - m_1$. The results for the benchmark cases of the dijet mother particle mass of 10 GeV and 40 GeV are shown in (a) and (b), respectively.

3.2 $h \to (b\bar{b}) + \not{E}_\mathrm{T}$

The background and the benchmark model for this mode are the same as the $h \to (jj) + \not{E}_\mathrm{T}$ case discussed in the previous section. The signal event is required to contain two b-tagged jets. The b-tagging efficiency is conservatively chosen to be 80%, and the charm mis-tagging rate and the light flavor mis-tagging rate are set to be 9% and 1%, respectively. Similarly, we use the likelihood function of the $m_{b\bar{b}}$-$\not{E}_\mathrm{T}$ distribution to derive the exclusive limit.
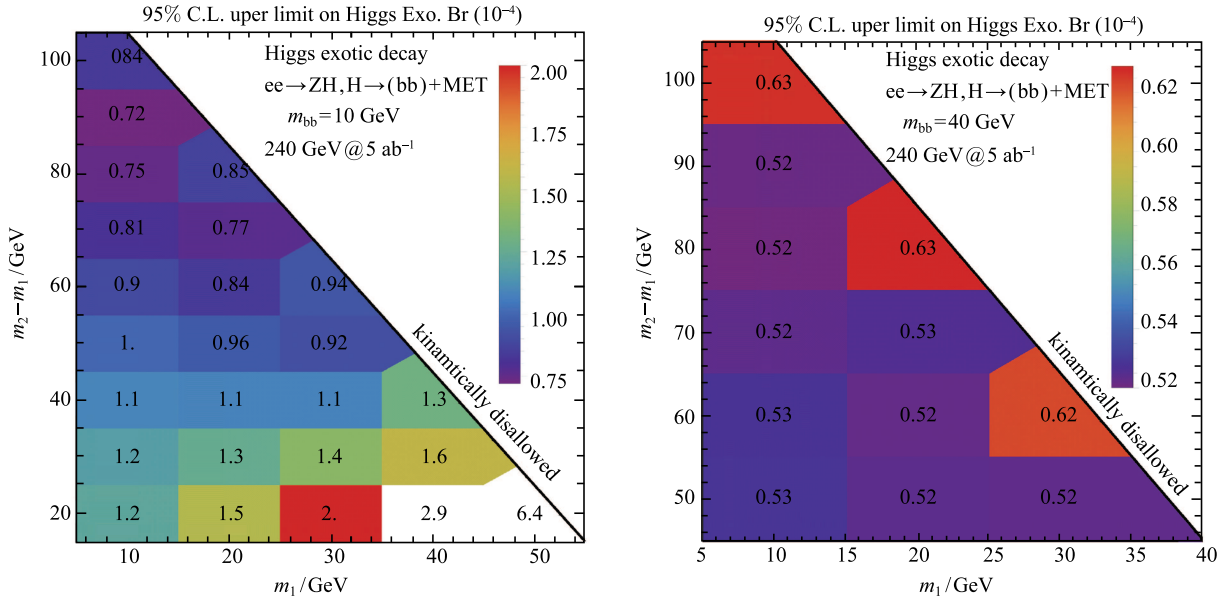

Fig. 5. (color online) The 95% C.L. upper limit on the Higgs exotic decay branching fractions into $(jj) + \not{E}_\mathrm{T}$ for various lightest detector-stable particle with mass m_1 and mass splittings $m_2 - m_1$. The results for the benchmark cases of a dijet mother particle mass of 10 GeV and 40 GeV are shown in (a) and (b), respectively.

We show the 95% C.L. exclusion limit in Fig. 5 in the plane of X_1, mass m_1, and the mass splitting between X_2 and X_1, m_2-m_1, for two benchmark intermediate scalar masses of 10 GeV (a) and 40 GeV (b). In most of the parameter space, the Higgs branching fraction to this exotic decay channel $h\to(b\bar{b})+\not{E}_T$ can be excluded to the level of $5\times10^{-5}\sim1.5\times10^{-4}$. The features for various kinematical regions are also similar to the analysis in the previous section. The limits are roughly a factor of 4 better than $h\to(jj)+\not{E}_T$ across the whole parameter region, due to the b-tagging reducing the flavor universal quark jets background. In the highest sensitivity benchmark points, the 95% C.L. exclusion bound can reach 6×10^{-5} (e.g., $m_1=10$ GeV, $m_2=60\sim100$ GeV, $m_s=40$ GeV). This impressive result nearly reaches the statistical limit of CEPC, after folding in a factor 0.64 on signal strength from the requirement of double b-tagging.

3.3 $h\to jj+\not{E}_T$ and $h\to b\bar{b}+\not{E}_T$

Although the final states of these channels are the same as the $h\to(jj)+\not{E}_T$ and $h\to(b\bar{b})+\not{E}_T$ cases discussed in the previous sections, the distribution of the kinetic variables is quite different since there is no dijet resonance in this case. We assume the intermediate particle (e.g., scalar s) to be very heavy so that the decay of the X_2 can be fully described by a four-fermion contact operator. Similarly, we use the likelihood function of the $m_{b\bar{b}}$-$\not{E}_T$ distribution to derive the exclusive limit. The results are shown in Fig. 6 in the plane of X_1, mass m_1, and the mass splitting between X_2 and X_1, m_2-m_1, for $h\to jj+\not{E}_T$ (a) and $h\to b\bar{b}+\not{E}_T$ (b). Comparing with the Higgs exotic decays with intermediate resonance in the previous section, the exclusion limits on the branching fraction are only slightly worse in the bulk region of the parameter space, reaching generally $3\times10^{-4}\sim8\times10^{-4}$ and $2\times10^{-4}\sim4\times10^{-4}$ for $h\to jj+\not{E}_T$ and $h\to b\bar{b}+\not{E}_T$, respectively.

From the exclusion limits shown in Fig. 6, we find that when the mass splitting m_2-m_1 is around 80 GeV, the future lepton colliders have the strongest sensitivities on these Higgs exotic channels, reaching around 3.1×10^{-4} and 1.6×10^{-4} for $h\to jj+\not{E}_T$ and and $h\to b\bar{b}+\not{E}_T$, respectively. When X_1 is light and m_2-m_1 is large, the energy is shared by the two jets and the X_1. Consequently, when the mass splitting m_2-m_1 is around 80 GeV, the dijet invariant mass will be around 40~60 GeV, falling in the "valley" of low SM background as shown in Fig. 3. For heavier X_1, the MET will be lower due to less momentum available for the LSP. The optimal limits will be reached for an even smaller mass splitting. The $b\bar{b}+\not{E}_T$ case has a higher sensitivity again by roughly a factor of two since the b-tagging suppresses the SM background.
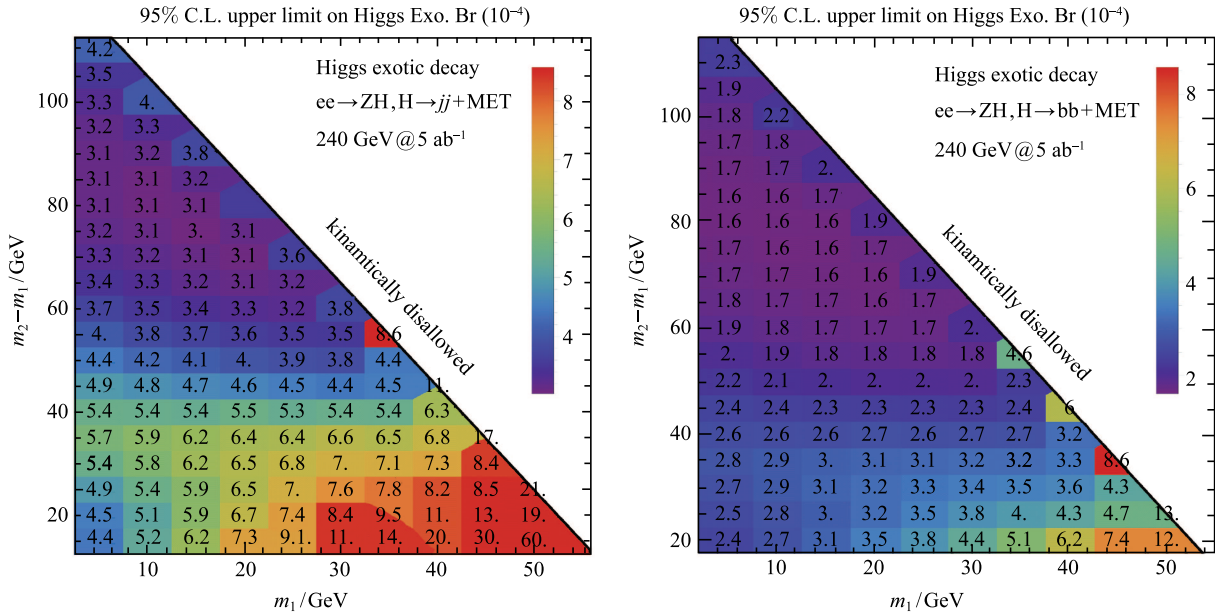

Fig. 6.   (color online) The 95% C.L. upper limit on the Higgs exotic decay branching fractions into $jj+\not{E}_T$ (a) and $b\bar{b}+\not{E}_T$ (b) for various lightest detector-stable particle mass m_1 and mass splittings m_2-m_1.

3.4 $h\to(jj)(jj)$, $h\to(c\bar{c})(c\bar{c})$ and $h\to(b\bar{b})(b\bar{b})$

For this class of Higgs exotic decays, we consider the scalar mediator (s), the pseudoscalar (a) and the vector (Z'^{μ}) mediator. We assume the effective interactions between the SM-like Higgs boson and the mediators are hss, haa and $hZ'^{\mu}Z'_{\mu}$, respectively. The (pseudo)scalar mediator can decay into dijet final states via $s\bar{f}f$ ($a\bar{f}\gamma_5 f$)

or $sG_{\mu\nu}G^{\mu\nu}$ ($aG_{\mu\nu}\tilde{G}^{\mu\nu}$) interactions. For the vector mediator case, we consider both the vector-like and right-handed interaction with the SM fermions.
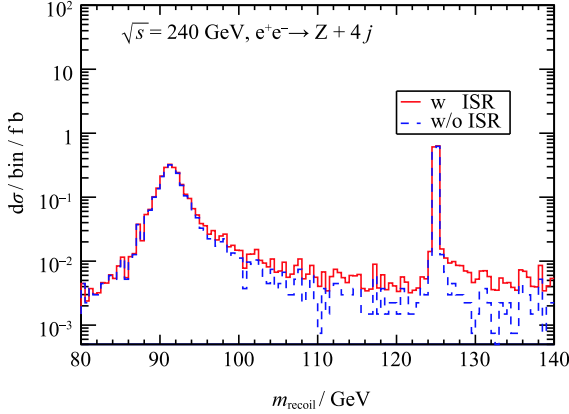

Fig. 7. (color online) The recoil mass distribution of the SM backgrounds for Z+4j. All cuts except for the recoil mass cut are applied. The red curve contains the contribution from $e^+e^- \to Z+4j+\gamma$.

In addition to the pre-selection cuts and the recoil mass cut, we require that there are at least four jets that satisfy

$$E_j > 5 \text{ GeV.} \tag{11}$$

The most important background from the SM is

$$e^+e^- \to Zh$$

with

$$Z \to l^+l^-, h \to jjjj, \tag{12}$$

where the four jets could be either from the hadronic decay of the SM vector bosons in $h \to VV^*$, or from $h \to jj$ with jet-splitting. We show the recoil mass distribution of the SM background with all but the recoil mass cut applied in Fig. 7. We also include in the red curves the background distribution with the inclusion of ISR effect. Its effect is negligibly small after the relatively large window of the recoil mass cut. We hence neglect the ISR effect in this analysis.

Another kinematical variable which is useful for separating the signal and background is

$$\delta m \equiv \min_{\sigma \in A_4} \left| m_{j_{\sigma(1)}j_{\sigma(2)}} - m_{j_{\sigma(3)}j_{\sigma(4)}} \right|. \tag{13}$$

With the combination which gives δm, we calculate the likelihood function of the $m_{j_1j_2} + m_{j_3j_4}$ versus δm distribution and get the 95% C.L. exclusive bound shown in Fig. 8. The chiral structure does not affect the result significantly. In the exclusion bounds, we only show the vector current result of the vector mediator.
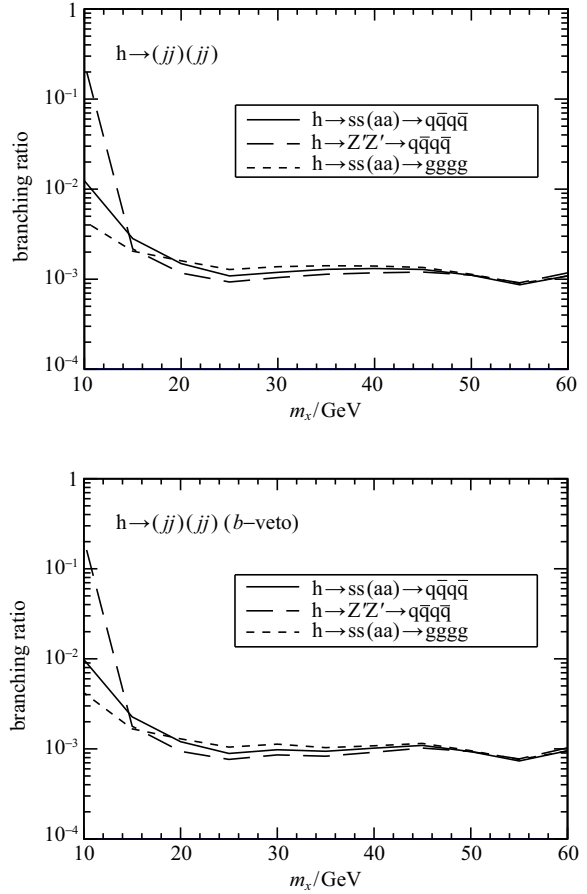

Fig. 8. The 95% C.L. exclusive bound of $Br(h \to (jj)(jj))$ (a) without and (b) with b-veto.

If the mediator decays to the light flavors (u,d,s,c,g) but not the bottom quark, a b-veto could be used to suppress the SM background. In this case, we require that there is no b-tagged jet in the final state. The b-veto does not increase the sensitivity significantly, as shown in Fig. 8(b), because the SM background is dominated by the $Z(h \to VV^* \to jjjj)$, which has a similar composition of quark flavors.

The future lepton collider with 5 ab^{-1} integrated luminosity could exclude 10^{-3} branching fractions of $h \to (jj)(jj)$ in a wide range of the mediator mass. We do not consider the mediator mass below 10 GeV as a different analysis strategy should then be taken because the jets are more likely to fail the separation cuts, manifested in the left-hand corner of Fig. 7.

The sensitivity in this channel is worse than in $h \to (jj) + \not{E}_T$ and $h \to jj + \not{E}_T$. This is because we miss the information of the correct combination of jets in the final state. The wrong combination of jets in the final state from the SM background will mimic the signal.

For the case of di-bottom pair resonances $h \to (b\bar{b})(b\bar{b})$ and di-charm pair resonances $h \to (c\bar{c})(c\bar{c})$, the simulation is nearly identical to the $h \to (jj)(jj)$ case.

We require at least three b-tagged jets and c-tagged jets in the final state, respectively. For the charm-tagging, we assume a tagging efficiency of 60% and mis-tag rate from b-jets 15% and light jets 10%. The relatively larger fake rate assumed here leads to slightly worse sensitivity for $h \to (c\bar{c})(c\bar{c})$ when comparing with $h \to (b\bar{b})(b\bar{b})$. The results are shown in Fig. 9. The future lepton collider with 5 ab^{-1} integrated luminosity could exclude branching fractions of $h \to (b\bar{b})(b\bar{b})$ and $h \to (c\bar{c})(c\bar{c})$ down to $3 \times 10^{-4} \sim 4 \times 10^{-4}$ and $7 \times 10^{-4} \sim 9 \times 10^{-4}$, respectively, in a wide range of the mediator mass.
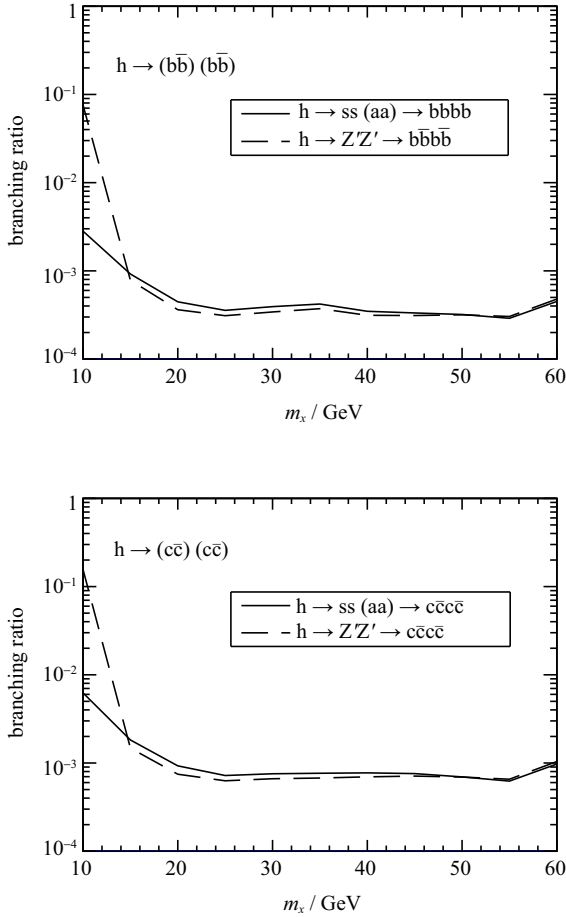

Fig. 9. The 95% C.L. exclusive bound on (a) $Br(h \to (b\bar{b})(b\bar{b}))$ and (b) $Br(h \to (c\bar{c})(c\bar{c}))$.

3.5 $h \to (\gamma\gamma)(\gamma\gamma)$

For this scenario, we consider the (pseudo)scalar mediator. In addition to the preliminary cuts, we require there are at least four hard photons that satisfy

$$E_\gamma > 10 \text{ GeV}. \qquad (14)$$

The most important background from the SM is

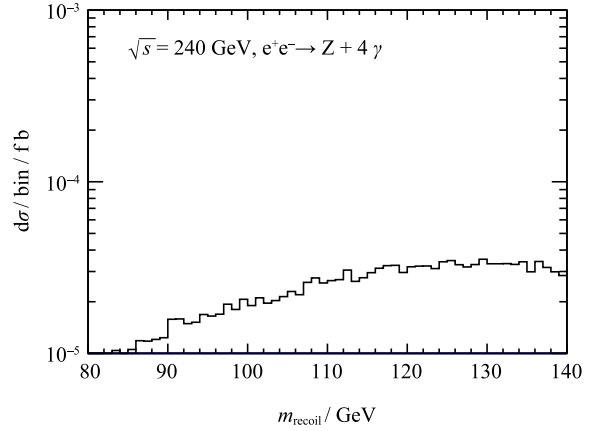$$e^+e^- \to Z + 4\gamma$$

with

$$Z \to l^+l^-. \qquad (15)$$

Fig. 10. The recoil mass distribution of the SM backgrounds for $Z + 4\gamma$. The R_m cut and all of the pre-selection cuts except for the recoil mass cut are applied.

We show the SM background distribution in the recoil mass after imposing all the other kinematical cuts in Fig. 10. The contribution from $e^+e^- \to Z + h + 2\gamma \to l^+l^- + 4\gamma$ is highly suppressed by the $h \to \gamma\gamma$ decay branching ratio [1]. The SM Z boson decaying into a four photon final state has a tiny branching ratio and thus it does not contribute. Therefore, there is no sizable resonance structure in the recoil mass distribution in the SM background of this channel, as shown in this figure.

Beyond the pre-selection cuts, the four photons should form two pairs of diphoton resonances with similar masses and thus we further require

$$R_m \equiv \min_{\sigma \in A_4} \left| \frac{m_{\gamma_{\sigma(1)}\gamma_{\sigma(2)}} - m_{\gamma_{\sigma(3)}\gamma_{\sigma(4)}}}{m_{\gamma_{\sigma(1)}\gamma_{\sigma(2)}} + m_{\gamma_{\sigma(3)}\gamma_{\sigma(4)}}} \right| < 0.1 \qquad (16)$$

for a signal event. The SM background is 0.14×10^{-3} fb. Around three signal events are needed to be excluded at 95% C.L. for 5 ab^{-1} integrated luminosity.

Table 1. The cut acceptances for the $h \to (\gamma\gamma)(\gamma\gamma)$ and the derived 95% C.L. limits on decay branching ratio $Br(h \to (\gamma\gamma)(\gamma\gamma))$ with 5 ab^{-1} integrated luminosity for various masses of the scalar mediator.

$m_{\text{med}}/$GeV	10	20	25	30	50
$sF_{\mu\nu}F^{\mu\nu}, aF_{\mu\nu}\tilde{F}^{\mu\nu}$	7.8%	33%	37%	41%	60%
$Br(h \to (\gamma\gamma)(\gamma\gamma))$ (10^{-4})	5.1	1.2	1.1	0.97	0.66

---

1) The cross section of $e^+e^- \to Z + h \to l^+l^- + 2\gamma$ is less than 40 ab and is severely suppressed by two more hard photons in the final state, so it is neglected here.

We tabulate the signal efficiency for various intermediate masses and show the derived 95% C.L. limits on this Higgs exotic branching fraction $Br(\mathrm{h} \to (\gamma\gamma)(\gamma\gamma))$ in Table 1. The signal acceptance for this analysis increases as the mediator mass increases, as a result of the requirement on the photon energy in Eq. (14). The limits can reach up to 4.7×10^{-4} on the exotic branching fractions of this channel for a mediator mass of 50 GeV.

3.6 $\mathrm{h} \to (jj)(\gamma\gamma)$

For this scenario, we consider the (pseudo)scalar mediator. In additional to the preliminary cuts, we require there are at least two hard photons and two hard jets that satisfy

$$E_{\gamma,j} > 10 \text{ GeV}. \tag{17}$$

The most important background from the SM is

$$\mathrm{e^+e^-} \to \mathrm{Z} + 2\gamma + 2j$$

with

$$\mathrm{Z} \to \mathrm{l^+l^-}. \tag{18}$$

The contribution from $\mathrm{e^+e^-} \to \mathrm{Z} + \mathrm{h} \to \mathrm{l^+l^-} + \mathrm{b\bar{b}} \to \mathrm{l^+l^-} + \mathrm{b\bar{b}} + 2\gamma$ is suppressed by the fine structure constant and the separation cut on y in Eq. (1). We show the SM background distribution in the recoil mass with the all but the recoil mass cut in Fig. 11. The background is mostly from $\mathrm{e^+e^-} \to \mathrm{ZZ} + 2\gamma$ where the photons are from the ISR. There is also a sizable contribution from $\mathrm{e^+e^-} \to \mathrm{ZZ}$ where one of the Z boson decays into a $q\bar{q}$ final state and the photons are from the final state radiation from the jets. We can find a small peak at the Z-pole in the recoil mass distribution in this figure.
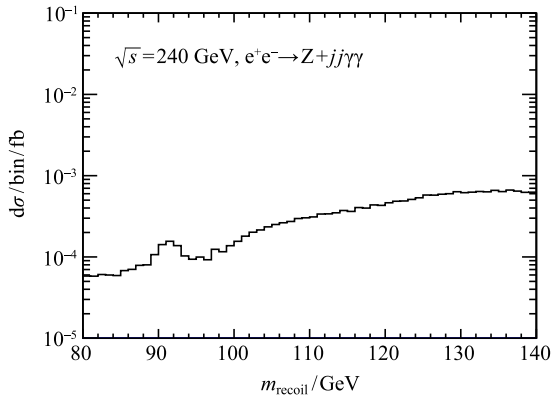

Fig. 11.   The recoil mass distribution of the SM backgrounds for $\mathrm{Z} + 2\gamma + 2j$. All but the recoil mass cut are applied.

We also require the dijet invariant mass and diphoton invariant mass to be close in value,

$$R_m \equiv \frac{|m_{jj} - m_{\gamma\gamma}|}{m_{jj} + m_{\gamma\gamma}} < 0.1 \tag{19}$$

to further suppress the background.

The SM background is 0.31×10^{-3} fb. Around four signal events are needed to be excluded at 95% C.L. for 5 ab^{-1} integrated luminosity.

Table 2.   The cut acceptances for the $\mathrm{h} \to (jj)(\gamma\gamma)$ and the derived 95% C.L. limits on decay branching ratio $Br(\mathrm{h} \to (jj)(\gamma\gamma))$ with 5 ab^{-1} integrated luminosity for various masses of the scalar mediator.

m_{med}/GeV	10	20	25	30	50
cut acceptance	10%	34%	39%	44%	66%
$Br(\mathrm{h} \to (jj)(\gamma\gamma))$ (10^{-4})	5.3	1.6	1.4	1.2	0.81

We tabulate the signal efficiency for various intermediate masses and show the derived 95% C.L. limits on this Higgs exotic branching fraction $Br(\mathrm{h} \to (jj)(\gamma\gamma))$ in Table 2. We can see the signal selection efficiency for this analysis increases as the mediator mass increases, as a result of the requirement on final state particle energies in Eq. (17). The limits can reach up to 5.6×10^{-4} on the exotic branching fractions of this channel for a mediator mass of 50 GeV.

4   Summary and outlook

We summarize the set of Higgs exotic decays in Table 3, including current collections and projections of LHC constraints, and limits from our study for the CEPC, ILC and FCC-ee. For the LHC constraints, we tabulate both the current limits and projected limits on these exotic decay channels from various references. Due to the subtleties in the projections at the LHC from possible systematics, we only quote the projected limits from studies with highest integrated luminosity and label them accordingly, instead of naively scaling these results to the projected luminosity of (HL-)LHC. The current LHC limits are collected in the second column, and the square brackets represent 7 and 8 TeV LHC results alone. The projections for HL-LHC are collected in the third column, where the limits for 100 fb^{-1} and 300 fb^{-1} are shown in parentheses and square brackets respectively. The reference for the current limits and projected limits are also included. For projections on the reaches of HL-LHC, it should be understood that they are from Ref. [25] unless specified otherwise. The limits for the case of the ILC and FCC-ee are extrapolated from our CEPC analyses in Section 3 following the running scenario discussion in Section 2, assuming the reach is dominated by statistics. The decay channels involving τ-leptons are extrapolated and validated by our preliminary simulation, assuming a 40% τ-tagging efficiency with more background considered. We mark these extrapolated limits with an asterisk.

Table 3.　The current and projected limits on selected Higgs exotic decay modes for the (HL-)LHC, CEPC, ILC, and FCC-ee. Throughout our analysis, we assume SM production rates for the Higgs boson. The current LHC limits are collected in the second column, with the square brackets indicating 7 and 8 TeV LHC results alone. The projections for the HL-LHC are collected in the third column, where the limits for 100 fb^{-1} and 300 fb^{-1} alone are shown in parentheses and square brackets respectively. The references for the current limits and projected limits are included; for projections on the HL-LHC limits we omit the references if they are from Ref. [25]. We also omit the references for projections on the future lepton collider programs if the results are from this study. Limits extracted from related searches with reasonable assumptions are marked with asterisks following the results with details explained in the text. For more details about the benchmark parameter choices for some of the decay modes, see discussion in the main text.

decay mode	95% C.L. limit on Br				
	LHC	HL-LHC	CEPC	ILC	FCC-ee
$\not{E}_{\rm T}$	0.23 [49, 50]	0.056 [12–14]	0.0028 [16]	0.0025 [17]	0.005 [18]
$(b\bar{b}) + \not{E}_{\rm T}$	–	[0.2]	$1{\times}10^{-4}$	$2{\times}10^{-4}$	$5{\times}10^{-5}$
$(jj) + \not{E}_{\rm T}$	–	–	$5{\times}10^{-4}$	$5{\times}10^{-4}$	$2{\times}10^{-4}$
$(\tau^+\tau^-) + \not{E}_{\rm T}$	–	[1]	$8{\times}10^{-4}*$	$1{\times}10^{-3}$	$3{\times}10^{-4}$
$b\bar{b} + \not{E}_{\rm T}$	–	[0.2] [39]	$3{\times}10^{-4}$	$4{\times}10^{-4}$	$1{\times}10^{-4}$
$jj + \not{E}_{\rm T}$	–	–	$5{\times}10^{-4}$	$7{\times}10^{-4}$	$2{\times}10^{-4}$
$\tau^+\tau^- + \not{E}_{\rm T}$	–	–	$8{\times}10^{-4}*$	$1{\times}10^{-3}$	$3{\times}10^{-4}$
$(b\bar{b})(b\bar{b})$	1.7 [51]	(0.2)	$4{\times}10^{-4}$	$9{\times}10^{-4}$	$3{\times}10^{-4}$
$(c\bar{c})(c\bar{c})$	–	(0.2)	$8{\times}10^{-4}$	$1{\times}10^{-3}$	$3{\times}10^{-4}$
$(jj)(jj)$	–	[0.1]	$1{\times}10^{-3}$	$2{\times}10^{-3}$	$7{\times}10^{-4}$
$(b\bar{b})(\tau^+\tau^-)$	[0.1]* [52]	[0.15]	$4{\times}10^{-4}*$	$6{\times}10^{-4}$	$2{\times}10^{-4}$
$(\tau^+\tau^-)(\tau^+\tau^-)$	[1.2]* [53]	[0.2 ∼ 0.4]	$1{\times}10^{-4}*$	$2{\times}10^{-4}$	$5{\times}10^{-5}$
$(jj)(\gamma\gamma)$	–	[0.01]	$1{\times}10^{-4}$	$2{\times}10^{-4}$	$3{\times}10^{-5}$
$(\gamma\gamma)(\gamma\gamma)$	[$7{\times}10^{-3}$] [54]	$4{\times}10^{-4}*$	$1{\times}10^{-4}$	$1{\times}10^{-4}$	$3{\times}10^{-5}$

Similar to the lepton collider, the LHC reach can depend on model parameters. While a comparison of the reach throughout the full parameter space is possible, it is tedious and not illuminating. We choose to focus on comparison for particular benchmark points, which is good enough to demonstrate the qualitative difference between the LHC and future lepton colliders. These choices are to make the limits more or less representative of the intermediate ("average") limits across wide parameter regions without being in the extremely good or bad kinematical points.

The LHC reach for $(b\bar{b})(\tau^+\tau^-)$ and $(\tau^+\tau^-)(\tau^+\tau^-)$ is extrapolated from the $(b\bar{b})(\mu^+\mu^-)$ and $(\tau^+\tau^-)(\mu^+\mu^-)$ searches, respectively, assuming $Br(a \to \tau^+\tau^-)/Br(a \to \mu^+\mu^-) = m_\tau^2/m_\mu^2$. For the process of h $\to aa \to (b\bar{b})(\mu^+\mu^-)$ with $m_a = 30$ GeV, the HL-LHC projected sensitivity is 5×10^{-5} [55], translating into a limit on h $\to aa \to (b\bar{b})(\tau^+\tau^-)$ of 0.02, better than the projected direct search limit on this channel from Ref. [25].

Photons are one of the "clean" objects in the LHC collider environment and the large statistics at the HL-LHC can constrain decays with photons to good precision. However, these is some discrepancy between the theoretical projections in Ref. [25] of $3{\times}10^{-5}$ at 300 fb^{-1}, and the extrapolation from the current limit at the 8

TeV LHC [54]. We choose to use the more conservative extrapolation by us and thus put an asterisk after the projected limit in this summary table.

For the decay topologies involving intermediate resonant particles, we choose the intermediate particle to be a pseudoscalar with a mass of 30 GeV as a benchmark, which applies to the $(b\bar{b})(b\bar{b})$, $(c\bar{c})(c\bar{c})$, $(jj)(jj)$, $(b\bar{b})(\tau^+\tau^-)$, $(\tau^+\tau^-)(\tau^+\tau^-)$, $(jj)(\gamma\gamma)$, and $(\gamma\gamma)(\gamma\gamma)$ decay channels. For a decay topology of h $\to 2 \to 3 \to 4$ where intermediate resonances are involved, we choose the lightest stable particle mass to be 10 GeV, the mass splitting to be 40 GeV and the intermediate resonance mass to be 10 GeV, which applies to $(b\bar{b})+\not{E}_{\rm T}$, $(jj)+\not{E}_{\rm T}$, $(\tau^+\tau^-)+\not{E}_{\rm T}$. For a decay topology of h $\to 2 \to (1+3)$, we choose the lightest stable particle mass to be 10 GeV and the mass splitting to be 40 GeV, which applies to $b\bar{b} + \not{E}_{\rm T}$, $jj + \not{E}_{\rm T}$, $\tau^+\tau^- + \not{E}_{\rm T}$. For the Higgs invisible decays, we take the best limits in the running scenario ECFA16-S2 amongst the Zh associated production and VBF search channels [12–14].

For the Higgs invisible decays at lepton colliders, we quote the limits from current studies [16–18]. These limits do not depend on the invisible particle mass using the recoil mass technique at lepton colliders.
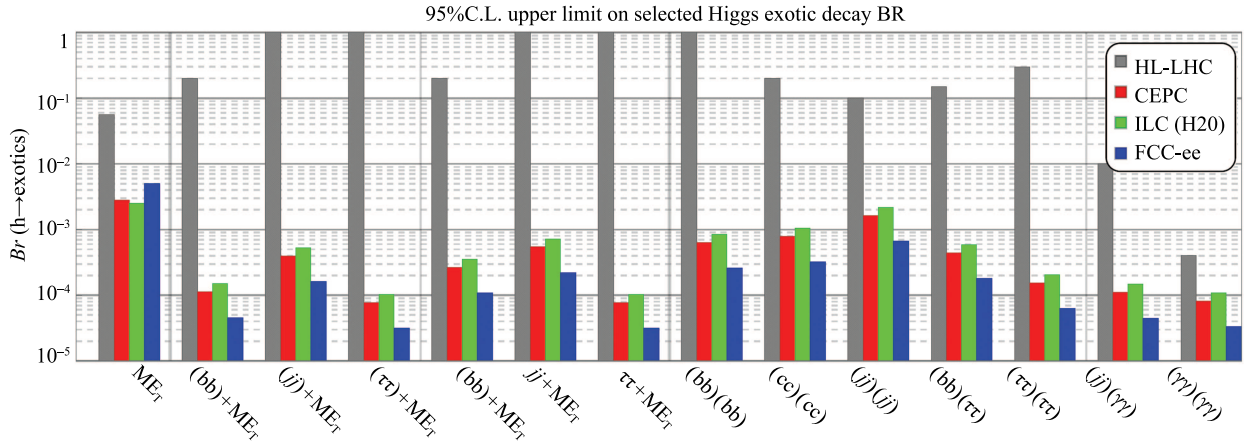
Fig. 12. (color online) The 95% C.L. upper limit on selected Higgs exotic decay branching fractions at HL-LHC, CEPC, ILC and FCC-ee. The benchmark parameter choices are the same as in Table 3. We put several vertical lines in this figure to divide different types of Higgs exotic decays.

From this summary in Table 3 and the corresponding Fig. 12, we can clearly see the improvement in exotic decays from the lepton collider Higgs factories. These exotic Higgs decay channels are selected such that they are hard to be constrained at the LHC but important for probing BSM decays of the Higgs boson. The improvements on the limits of the Higgs exotic decay branching fractions vary from one to four orders of magnitude for these channels. The lepton colliders can improve the limits on the Higgs invisible decays beyond the HL-LHC projection by one order of magnitude, reaching the SM invisible decay branching fraction of 0.12% from $h \to ZZ^* \to \nu\bar{\nu}\nu\bar{\nu}$ [56]. For the Higgs exotic decays into hadronic particle plus missing energy, $(b\bar{b}) + \not{E}_T$, $(jj) + \not{E}_T$ and $(\tau^+\tau^-) + \not{E}_T$, the future lepton colliders improve on the HL-LHC sensitivity for these channels by roughly four orders of magnitude. This great advantage benefits a lot from low QCD background and the Higgs tagging from recoil mass technique at future lepton colliders. As for the Higgs exotic decays without missing energy, the improvement varies between two to three orders of magnitude, except for the one order of magnitude improvement for the $(\gamma\gamma)(\gamma\gamma)$ channel. Being able to reconstruct the Higgs mass from the final state particles at the LHC does provide additional signal-background discrimination power and hence the future lepton colliders improvement on Higgs exotic decays without missing energy is less impressive than for those with missing energy. Furthermore, as discussed earlier, leptons and photons are relatively clean objects at the LHC and the sensitivity at the LHC on these channels will be very good. Future lepton colliders complement the HL-LHC for hadronic channels and channels with missing energies.

There are many more investigations to be carried out under the theme of Higgs exotic decays. For our study, we take the cleanest channel of $e^+e^- \to ZH$ with $Z \to l^+l^-$ and h →exotics up to four-body final state, but further inclusion of the hadronic decaying spectator Z-boson and even invisible decays of the Z-boson would definitely improve the statistics and consequently result in better limits. As a first attempt to evaluate the Higgs exotic decay program at future lepton colliders, we do not include the case of very light intermediate particles whose decay products will be collimated, but postpone this for future study when the detector performance is more clearly defined. There are many more exotic Higgs decay modes to consider, such as Higgs decaying to a pair of intermediate particles with un-even masses [25], Higgs CP property measurements from its decay differential distributions [57–60], flavor violating decays, decays to light quarks [61], decays into meta-stable particles, and complementary Higgs exotic productions [62]. Our work is a first systematic study evaluating the physics potential of future lepton colliders to probe Higgs exotic decays. More work will be needed to obtain a complete picture.

References

1   G. Aad et al (ATLAS Collaboration), Phys. Lett. B, **716**: 1–29 (2012)
2   S. Chatrchyan et al (CMS Collaboration), Phys. Lett. B, **716**: 30–61(2012)
3   R. A. Flores and M. Sher, Annals Phys., **148**: 95 (1983)
4   J. F. Gunion and H. E. Haber, Nucl. Phys. B, **272**: 1 (1986)
5   A. Djouadi, Phys. Rept., **459**: 1–241 (2008)
6   B. Gripaios, A. Pomarol, F. Riva et al, JHEP, **04**: 70 (2009)
7   N. Arkani-Hamed, S. Dimopoulos, and G. R. Dvali, Phys. Rev. D, **59**: 086004 (1999)
8   L. Randall and R. Sundrum, Phys. Rev. Lett., **83**: 3370–3373 (1999)
9   L. Randall and R. Sundrum, Phys. Rev. Lett., **83**: 4690–4693 (1999)
10 H. Georgi and S. L. Glashow, Phys. Rev. Lett., **32**: 438–441 (1974)
11 S. Dawson et al., arXiv:1310.8361
12 CMS Collaboration, arXiv:1307.7135
13 https://cds.cern.ch/record/2221747/files/DP2016_064.pdf, retrieved 4th October 2016
14 http://cds.cern.ch/record/1611186/files/ATL-PHYS-PUB-2013-014.pdf, retrieved 17th October 2013
15 http://cds.cern.ch/record/1956710/files/ATL-PHYS-PUB-2014-016.pdf, retrieved 21st October 2014
16 http://cepc.ihep.ac.cn/preCDR/main_preCDR.pdf,   retrieved 4th May 2015
17 K. Fujii et al., arXiv:1506.05992
18 M. Bicer et al (TLEP Design Study Working Group Collaboration), JHEP, **01**: 164 (2014)
19 S. Weinberg, Physica A, **96**: 327–340 (1979)
20 W. Buchmuller and D. Wyler, Nucl. Phys. B, **268**: 621–653 (1986)
21 B. Grzadkowski, M. Iskrzynski, M. Misiak et al, JHEP, **10**: 85 (2010)
22 J. Ellis, V. Sanz and T. You, JHEP, **03**: 157 (2015)
23 A. Biekötter, A. Knochel, M. Krämer et al, Phys. Rev. D, **91**: 055029 (2015)
24 R. Contino, A. Falkowski, F. Goertz et al, JHEP, **07**: 144 (2016)
25 D. Curtin, R. Essig, S. Gori et al, Phys. Rev. D, **90**: 075004 (2014)
26 D. de Florian et al, arXiv:1610.07922
27 B. Patt and F. Wilczek, arXiv: hepph/0605188
28 A. Arbey, M. Battaglia, and F. Mahmoudi, Eur. Phys. J. C, **72**: 2169 (2012)
29 P. S. Bhupal Dev, S. Mondal, B. Mukhopadhyaya et al, JHEP, **09**: 110 (2012)
30 T. Han, Z. Liu, and A. Natarajan, JHEP, **11**: 8 (2013)
31 S. Banerjee, P. S. B. Dev, S. Monda et al, JHEP, **10**: 221 (2013)
32 M. R. Buckley, D. Hooper, and J. Kumar, Phys. Rev. D, **88**: 063532 (2013)
33 K. Hagiwara, S. Mukhopadhyay, and J. Nakamura, Phys. Rev. D, **89**: 015023 (2014)
34 G. Bélanger, G. Drieu La Rochelle, B. Dumont et al, Phys. Lett. B, **726**: 773–780 (2013)
35 A. Pierce, N. R. Shah, and K. Freese, arXiv:1309.7351
36 J. Cao, C. Han, L. Wu et al, JHEP, **05**: 56 (2014)
37 T. Han, Z. Liu, and S. Su, JHEP, **08**: 93 (2014)
38 J. Huang, T. Liu, L.-T. Wang et al, Phys. Rev. D, **90**: 115006 (2014)
39 J. Huang, T. Liu, L.-T. Wang et al, Phys. Rev. Lett., **112**: 221803 (2014)
40 J. Fan, M. Reece, and J. T. Ruderman, JHEP, **11**: 12 (2011)
41 Q. Xiu, H. Zhu, X. Lou et al, Chin. Phys. C, **40**: 053001 (2016)
42 M. Greco, T. Han, and Z. Liu, Phys. Lett. B, **763**: 409–415 (2016)
43 R. Essig et al., arXiv:1311.0029
44 P. J. Fox, J. Liu, D. Tucker-Smith et al, Phys. Rev. D, **84**: 115006 (2011)
45 Z. Chacko, H.-S. Goh, and R. Harnik, Phys. Rev. Lett., **96**: 231802 (2006)
46 Q.-F. Sun, F. Feng, Y. Jia et al, arXiv:1609.03995
47 Y. Gong, Z. Li, X. Xu et al, arXiv:1609.03955
48 J. Alwall, R. Frederix, S. Frixione et al, JHEP, **1407**: 79 (2014)
49 G. Aad et al (ATLAS Collaboration), JHEP, **11**: 206 (2015)
50 V. Khachatryan et al (CMS Collaboration), arXiv:1610.09218
51 M. Aaboud et al (ATLAS Collaboration), Eur. Phys. J. C, **76**: 605 (2016)
52 https://cds.cern.ch/record/2135985/files/HIG-14-041-pas.pdf, retrieved 3rd March 2016
53 G. Aad et al (ATLAS Collaboration), Phys. Rev. D, **92**: 052002 (2015)
54 G. Aad et al (ATLAS Collaboration), Eur. Phys. J. C, **76**: 210 (2016)
55 D. Curtin, R. Essig, and Y.-M. Zhong, JHEP, **06**: 25 (2015)
56 J. R. Andersen et al, arXiv:1307.1347
57 R. Harnik, A. Martin, T. Okui et al, Phys. Rev. D, **88**: 076009 (2013)
58 G. Li, H.-R. Wang, and S.-h. Zhu, Phys. Rev. D, **93**: 055038 (2016)
59 N. Craig, J. Gu, Z. Liu et al, JHEP, **03**: 50 (2016)
60 G. Li, Y.-n. Mao, C. Zhang et al, arXiv:1611.08518
61 J. Gao, arXiv:1608.01746
62 Q.-H. Cao, H.-R. Wang, and Y. Zhang, Chin. Phys. C, **39**: 113102 (2015)
63 https://cds.cern.ch/record/1983181/files/HIG-14-024-pas.pdf, retrieved 27th January 2015